Coordinate conversion and switching correction to reduce vessel heading related errors in high-latitude navigation

Yufei Wang* Lokukaluge P. Perera* Bjørn-Morten Batalden*

*UiT The Arctic University of Norway, Tromsø, 9037 Norway
(yufei.wang@uit.no; prasad.perera@uit.no; bjorn.batalden@uit.no)

Abstract: Considering the distortion errors of projected coordinates and the switching property of vessel heading, coordinate conversion and switching correction methods are proposed to modify a kinematic motion model and the Unscented Kalman Filter (UKF). The coordinate conversion method utilizes the grid convergence from a Universal Transverse Mercator (UTM) projection to correct the vessel heading. The switching correction is embedded in the UKF so that the innovations of vessel heading can be calculated correctly. The simulation results demonstrate that the proposed modifications in both model and algorithm can generate more accurate estimated vessel states from two simulated maneuvers. Since a reliable estimation of vessel maneuvers is the prerequisite in many intelligent systems that support various decision-making processes in maritime transportation, the proposed modifications can be therefore implemented into these systems to support navigation safety in high latitude areas.

Keywords: vessel state estimation, kinematic motion model, Unscented Kalman Filter, UTM coordinate system, navigation in high latitudes, circular data.

1. INTRODUCTION

The recent development in industrial digitization brings new opportunities and challenges to the traditional maritime industry. Many latest intelligence systems supported by artificial intelligence and big data become highly involved in various maritime applications, i.e., energy efficiency, equipment maintenance, navigation, and accident prevention, etc (Munim et al., 2020). Since future vessels will be navigated by intelligent systems, the threshold for navigation errors should be minimized, especially in high latitudes. On the other hand, human navigation activities in high latitudes have an increasing trend in recent years. With global warming and the gradual disappearance of the Arctic ice caps, the potential of Arctic shipping routes is being constantly highlighted (Aksenov et al., 2017).

As for intelligence systems to support ship navigation, safety can be an important factor. It is imperative to obtain reliable navigation data sets which are related to the vessel's maneuvering behaviors for the same purpose. These data sets can be used to estimate vessel states online, and the accuracy of estimated states needs to be guaranteed since poor quality of estimated states can cause the wrong prediction of vessel behaviors and finally lead to collisions or near-miss situations. Maneuvering behavior of vessels can be described by kinematic motion models in several studies (Li and Jilkov, 2003; Perera, 2017; Wang et al., 2022), and navigation states of vessels can be estimated by Kalman filter-based (KF) techniques with relatively high accuracy. However, as an implicit assumption that measured positions used in most kinematic motion models are actually the projected coordinates of the raw latitude/longitude data from GNSS systems, where the

UTM coordinate system has generally been used. Similar processing methods which use the UTM coordinate system in maritime research studies are also presented (Mu et al., 2019; Kim et al., 2022). The projected coordinates can introduce larger distortion errors in high-latitude areas, especially if the models are associated with heading measurements that can cause various erroneous conditions in state estimation. Consequently, a direct implementation of kinematic motion models in high latitudes can be problematic due to the same reasons.

Another factor that is usually omitted in applications of ship maneuvering is that the measured heading belongs to circular data (Philipp, 2009), which is different from other non-circular data, such as positions and velocities. Measured headings from advanced optical gyroscopes can show the switching property so that the readings can jump discontinuously from 0 to $360°$ when the ship's actual heading measurements are close to true north. The measurements of the discontinuous heading (i.e., varying among $0°+$ and $360°-$ values) can finally cause the estimation algorithms to diverge during vessel operations in such regions. There are several modified methods to handle the circular data, such as the quaternion-based estimation (Zhang et al., 2012) and the Invariant Extended Kalman Filter (Barrau, 2015). The distinctive feature of these methods is the representation of circular data to the unit quaternions and the Lie groups, respectively.

This paper proposes a novel methodology, i.e., coordinate conversion and switch correction method that work on the kinematic motion model with the UKF algorithms as a solution to the above-mentioned problem. These modifications can be conveniently applied to the same

model and estimation algorithm. Simulated or actual vessel maneuvers in high-latitude areas can use the proposed methodology to improve their navigation integrity. The remainder is organized as follows: Section 2 introduces the utilized coordinate conversion method of the UTM; the kinematic motion model is presented in Section 3; Section 4 describes the UKF algorithms; Section 5 shows the simulation settings and results; the conclusion and plans in next step are summarized in the final.

2. UTM COORDINATE CONVERSION

The UTM coordinate system is a commonly used projection coordinate system that can represent geographic positions in a Cartesian coordinate system. This system has extensively been used in ship navigation. The mechanism of the UTM projection is roughly shown in Fig. 1, and the details can be referred to Osborne (2013).
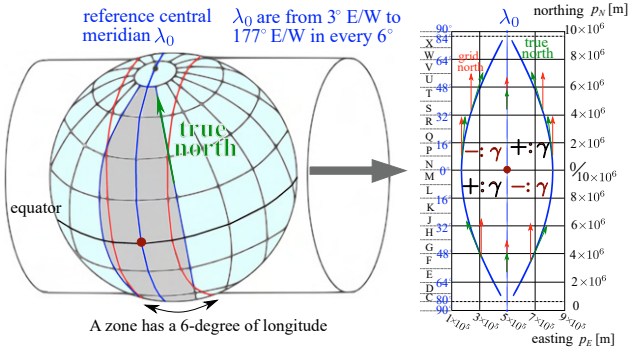

Fig. 1. The schema of UTM projection and coordinate system. There are 60 divided zones in total.

There are various methods that convert latitude and longitude (ϕ, λ) into northing and easting (p_N, p_E) in the UTM system. In this study, the method proposed by Kawase (2012) which consists of (2) to (11) is used since it is more convenient for computer programming. This methodology, i.e., the coordinate conversion method, is based on the WGS84 spatial reference system that describes the Earth as an oblate spheroid along the north-south axis with an equatorial radius a and a flattening f. Some preliminary constant parameters based on a and f can be calculated at first.

$$a = 6378.137[km]; \; 1/f = 298.257223563 \quad (1)$$

$$n = \frac{f}{2-f}; \; A = \frac{a}{1+n}\left(1 + \frac{n^2}{4} + \frac{n^4}{64} + \cdots\right) \quad (2)$$

$$\alpha_1 = \frac{1}{2} - \frac{2}{3}n^2 + \frac{5}{16}n^3; \alpha_2 = \frac{13}{48}n^2 - \frac{3}{5}n^3; \alpha_3 = \frac{61}{240}n^3 \quad (3)$$

The origin of the projected area lies in the intersection of the equator and the reference central meridian λ_0 (see Fig. 1). The point scale at the reference central meridian k_0 is specified to be 0.9996. To avoid negative position values, the origin of northing N_0 is set to 0[km] in the northern hemisphere and 10000[km] in the southern hemisphere. The origin of easting E_0 starts with 500[km]. With a measured ϕ and λ, p_N, p_E, local point scale k, and grid convergence γ can be calculated as:

$$p_N = N_0 + k_0 A\left(\xi' + \sum_{j=1}^{3} \alpha_j \sin\left(2j\xi'\right)\cosh\left(2j\eta'\right)\right) \quad (4)$$

$$p_E = E_0 + k_0 A\left(\eta' + \sum_{j=1}^{3} \alpha_j \cos\left(2j\xi'\right)\sinh\left(2j\eta'\right)\right) \quad (5)$$

$$k = \frac{k_0 A}{a}\sqrt{\left(1 + \left(\frac{1-n}{1+n}\tan\phi\right)^2\right)\frac{\sigma^2 + \tau^2}{t^2 + \cos^2\left(\lambda - \lambda_0\right)}} \quad (6)$$

$$\gamma = \tan^{-1}\left(\frac{\tau\sqrt{1+t^2} + \sigma \, t \, \tan\left(\lambda - \lambda_0\right)}{\sigma\sqrt{1+t^2} - \tau \, t \, \tan\left(\lambda - \lambda_0\right)}\right) \quad (7)$$

where:

$$t = \sinh\left(\tanh^{-1}\left(\sin\phi\right) - \frac{2\sqrt{n}}{1+n}\tanh^{-1}\left(\frac{2\sqrt{n}}{1+n}\sin\phi\right)\right) \quad (8)$$

$$\xi' = \tan^{-1}\left(\frac{t}{\cos(\lambda - \lambda_0)}\right); \eta' = \tanh^{-1}\left(\frac{\sin\left(\lambda - \lambda_0\right)}{\sqrt{1+t^2}}\right) \quad (9)$$

$$\sigma = 1 + \sum_{j=1}^{3} 2j\alpha_j \cos\left(2j\xi'\right)\cosh\left(2j\eta'\right) \quad (10)$$

$$\tau = \sum_{j=1}^{3} 2j\alpha_j \sin\left(2j\xi'\right)\sinh\left(2j\eta'\right) \quad (11)$$

Grid convergence γ is the difference between true north and grid north, and the sign of γ is shown in Fig. 1. The value of γ is zero in the equator and the central meridian. As objects move away from these axes, γ increases and will reach a higher value in high-latitude areas. Local point scale k in the UTM projection is determined by the located ϕ and λ. A maximum value of k can reach 1.0010 at the zone boundaries in the equator, which indicates a projected distance falls short of the true scale by 1 unit in 1000. For general collision avoidance, this projection error can be neglected.

3. SHIP MOTION MODEL

A kinematic motion model—Constant Turn Rate and Acceleration (CTRA) model is used in this study to model ship maneuvering behavior. It is assumed that the center of gravity (CG) does not shift greatly during maneuvering. The relevant navigation states which describe the CG of a vessel are shown in Fig. 2. It should be noted that
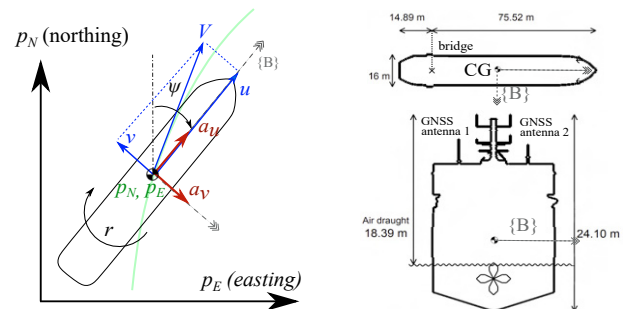

Fig. 2. The system states in the CTRA and the geometry information of the vessel used in the simulation

the heading as a system state in the CTRA model is based on the northing axis, i.e., grid north. As for the measurements, it is designed so that the vessel position, heading, yaw rate, and acceleration can be measured from on-board sensors as discrete-time signals. The measured position can be calibrated to the CG of the vessel. It is also assumed that IMUs are well located in the CG so that the measured accelerations do not contain any misaligned noises. In particular, optical gyroscopes are considered so that the measured heading is based on true north. Through the state-space representation method, a continuous-time system model and a discrete-time measurement model are considered and that can be written as:

$$\boldsymbol{x}(t) = [p_N, p_E, u, v, \psi, r, a_u, a_v]\,|_{(t)} \tag{12}$$

$$\dot{\boldsymbol{x}}(t) = f(\boldsymbol{x}(t)) + \boldsymbol{w_x} \tag{13}$$

$$= \begin{bmatrix} u(t)\cos(\psi(t)) - v(t)\sin(\psi(t)) \\ v(t)\cos(\psi(t)) + u(t)\sin(\psi(t)) \\ a_u(t) \\ a_v(t) \\ 0 \\ 0 \\ r(t) \\ 0 \end{bmatrix} + \boldsymbol{w_x} \tag{14}$$

where:

$$\boldsymbol{w_x} \sim \mathcal{N}\left(0,\, diag\left(\boldsymbol{Q} \in R^{8\times8}\right)\right)$$

$$\boldsymbol{z}[t_k] = [z_{p_N}, z_{p_E}, z_{au}, z_{av}, z_\psi, z_r]\,|_{[t_k]} \tag{15}$$

$$\boldsymbol{z}[t_k] = h(\boldsymbol{x}[t_k]) + \boldsymbol{w_z} = \begin{bmatrix} p_N[t_k] \\ p_E[t_k] \\ a_u[t_k] - v[t_k]\,r[t_k] \\ a_v[t_k] + u[t_k]\,r[t_k] \\ \psi[t_k] + \gamma \\ r[t_k] \end{bmatrix} + \boldsymbol{w_z} \tag{16}$$

where:

$$\boldsymbol{w_z} \sim \mathcal{N}\left(0,\, diag\left(\boldsymbol{R} \in R^{6\times6}\right)\right); t_k = k \cdot \Delta t \ (k = 0, 1, ...)$$

Both the system noise $\boldsymbol{w_x}$ and measurement noise $\boldsymbol{w_z}$ are assumed to be Gaussian noise, with their respective covariances being diagonal matrices. In the measurement model, p_N, p_E, and γ can be calculated based on the raw latitude/longitude data according to (4), (5), and (7). Since the change of γ is a small value in a local area, it is treated as a constant during the simulated maneuvers. Note that the calculated heading from the measurement models in (16) may not locate between 0° and 360°, which is inconsistent with z_ψ in (15). A modification towards the measurement innovations of heading is thus necessary.

4. STATE ESTIMATION ALGORITHM

The UKF is selected to estimate the states in the CTRA. The main feature of the UKF is that a set of sigma points ($\boldsymbol{s}$) with pre-defined weights (W) generated from unscented transformation can be used to approximate vessel states and error covariances. The calculation of Jacobians is not required in the UKF, and this is also a benefit for highly nonlinear systems. Since the system model consists of continuous differential equations, exact analytical solutions cannot be found in some situations, numerical methods are therefore developed to solve the prior states in prediction steps (Takeno and Katayama, 2012; Wang et al., 2022).

4.1 Switching correction of heading

After the prediction step, the filtering step will be executed. The posterior states are given by the combination of the prior estimates ($\hat{\boldsymbol{x}}_{t_k|t_{k-1}}$), Kalman gain ($K$), and the measurement innovation ($\boldsymbol{z}[t_k] - \hat{\boldsymbol{z}}_{t_k|t_{k-1}}$) which is also known as the measurement residual.

$$\hat{\boldsymbol{x}}_{t_k|t_k} = \hat{\boldsymbol{x}}_{t_k|t_{k-1}} + K\left(\boldsymbol{z}[t_k] - \hat{\boldsymbol{z}}_{t_k|t_{k-1}}\right) \tag{17}$$

$$\text{where: } \hat{\boldsymbol{z}}_{t_k|t_{k-1}} = h(\boldsymbol{s}[t_k])\,W$$

It should be noted that the difference operation of the measurement innovation in (17) is not suitable for the heading. Because of the switching property, the wrapping effect should be considered, e.g., the difference between 359° and 1° should be 2° instead of 358°. Therefore, a special treatment for the heading should be included. In this study, a switching correction is considered (see Alg. 1). This proposed methodology is based on the assumption that the yaw rate of ships is limited due to the low maneuverability compared with ground vehicles and aircraft. A sharp change of heading is thus unlike to happen for general ships, especially with large tonnages. A threshold value r_{lim} can be consequently applied to modify the innovations.

Algorithm 1
Switching correction for the heading in prediction step

Calculate the innovation of heading:
$$res_\psi = z_\psi[t_k] - \hat{\psi}_{t_k|t_{k-1}}$$

if $res_\psi \geq r_{lim}\,\Delta t$ **then**
    $res_\psi = res_\psi - 2\pi$
else if $res_\psi < -r_{lim}\,\Delta t$ **then**
    $res_\psi = res_\psi + 2\pi$
end if

After obtain the Kalman Gain K:
$$\hat{\psi}_{t_k|t_k} = \left\langle \hat{\psi}_{t_k|t_{k-1}} + K \cdot res_\psi \right\rangle$$
$$\text{where } \langle . \rangle := mod\left(mod\left(.,2\pi\right) + 2\pi, 2\pi\right)$$

4.2 Proposed error for heading

There are various types of errors based on the difference between actual and estimated states to evaluate the estimation accuracy of the respective algorithms. Obviously, the difference operation is not suitable for the switching properties of vessel heading. A vector-based error representation for vessel heading is used in this study (see Fig.3). The heading is converted into the heading vector which has the unit length and the initial point at the origin of the UTM coordinate. The magnitude of error is defined as the angle between two related heading vectors, where the angle can be calculated from the inner product. The sign of error is determined by the quadrants in UTM coordinate after a clockwise rotation of the heading vectors.

5. SIMULATION RESULTS AND DISCUSSION

Data sets from a ship bridge simulator that has the geographic data in the Svalbard area are used in this study. These data sets consist of two ship maneuvers, actual
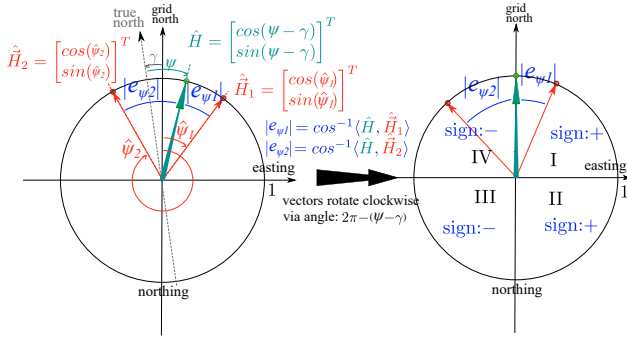
Fig. 3. The designed error representation for heading. Note that the actual heading (green vector) starts from true north; the estimated headings (2 red vectors) start from grid north.
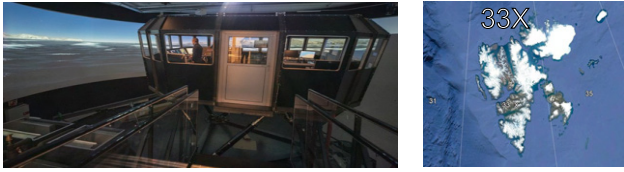

Fig. 4. The UiT ship bridge simulator. The satellite image of the Svalbard area is obtained from Google Earth.

vessel states and measurements (see Fig. 4). In order to verify the effectiveness of the proposed methodology, three scenarios are used to estimate the vessel states under the same initialized conditions (see table 1).

Table 1. Scenarios for state estimation

Config. name	grid convergence in the CTRA	switching correction in the UKF
Scenario 1	Yes	Yes
Scenario 2	Yes	No
Scenario 3	No	Yes

5.1 Simulated maneuvers

The simulated maneuvers are a straight line maneuver towards true north and a zigzag-like maneuver (see Fig. 5). The maneuver towards true north can actually happen in all navigation areas and provide highly discontinuous heading measurements that switch frequently between $0°+$ to $360°-$. Such a maneuver can be considered as an extreme situation, where the robustness of relevant state estimation algorithms can be degraded. The switching of heading can also happen in zigzag maneuvers. The zigzag maneuver showed in Fig. 5 suffers the switch of heading in time steps—t_1 to t_4. This maneuver can be frequently executed at high latitudes to avoid obstacles like ice conditions.

5.2 Parameter initialization

The related parameter initialization is shown in table 2. The variable δt is used as a temporal unit for the numerical calculation in the prediction steps. The parameters α, β, and κ are used in the UKF to tune the sigma points. The initialized state $\boldsymbol{x_0}$ can be generated from two historical measurements before the filter starts to work. The covariance matrices of both system and measurement noise ($\boldsymbol{Q}$
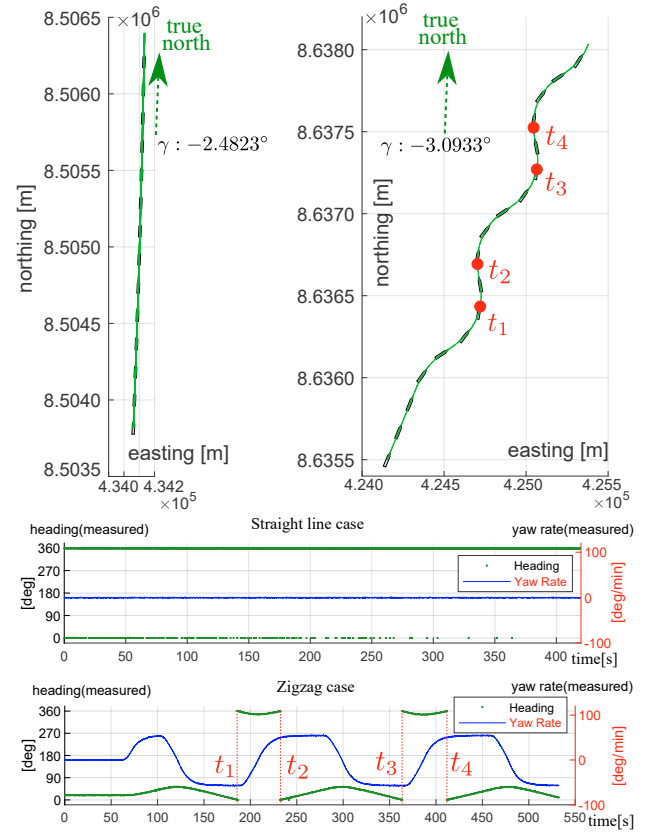

Fig. 5. The simulated straight line and zigzag maneuvers. The vessel position is recorded every 30 seconds. The measured heading and yaw rate are attached.

and $\boldsymbol{R}$) are assumed as diagonal matrices. The detail of the initialization process can be referred to Wang et al. (2022).

Table 2. Initilized parameters

Δt	$0.1[s]$	δt	$0.005[s]$
γ (line)	$-2.4823°$	γ (zigzag)	$-3.0933°$
r_{lim}	$50\pi/180[s^{-1}]$	α	0.3
β	2	κ	100
$\boldsymbol{Q}$	$diag(10^{-1}, 10^{-1}, 10^{-3}, 10^{-3},$ $10^{-5}, 10^{-5}, 10^{-1}\pi/180, 10^{-5}\pi/180)$		
$\boldsymbol{R}$	$diag(1, 1, (0.01)^2, (0.01)^2,$ $(0.5\pi/180)^2, (10^{-2}\pi/180)^2)$		
$\boldsymbol{x_0}$ (line)	$[8503821, 434061, 5.5, 0.1, 0, 0, 3.14, 0]$		
$\boldsymbol{x_0}$ (Zigzag)	$[8635500, 424155, 6.7, 0.9, 0, 0, 0.31, 0]$		

5.3 Simulation results

Figure 6 shows the Euclidean norm of the estimated position errors. In the straight line case, it can be seen clearly the larger estimated position error from Scenario 2 where the UKF does not contain the switch correction. In the zigzag case, there are occasions when the errors from Scenario 2 increase sharply. The moments that these occasions happen coincide with the time steps—t_1 to t_4 when the measured heading hits true north. However, during other time periods when the measured heading leaves away from true north, the errors from all of the scenarios are less than 1[m]. It can be also observed that the position errors from Scenario 1 and Scenario 3 are

similar in both maneuvering cases. The impact of grid convergence on the accuracy of position estimation in the CTRA is thus smaller. This can be interpreted as the predicted p_N and p_E will not change much without considering γ based on (14), and the measurements of p_N and p_E can also fix the errors in prediction steps.
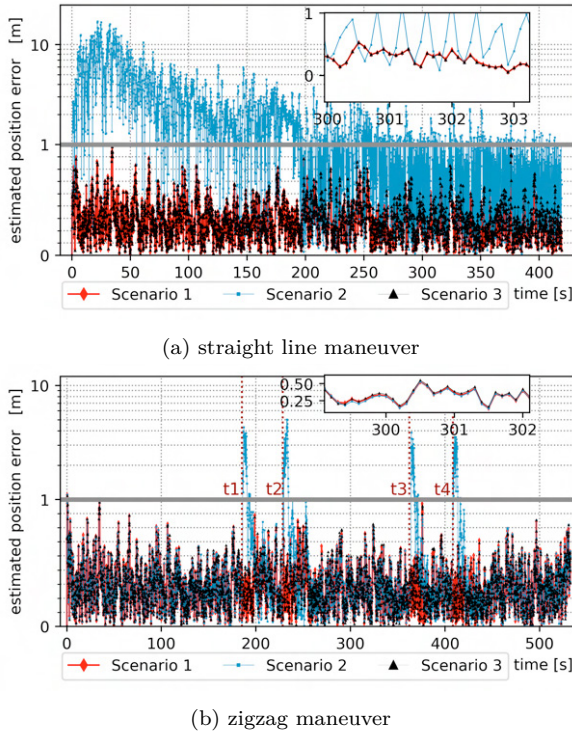

(a) straight line maneuver

(b) zigzag maneuver

Fig. 6. Euclidean norm of estimation position error. Errors above 1 [m] are plotted on log scale.

The estimated surge and sway velocities (u and v) are demonstrated in Fig.7, and it can be seen that the estimates from Scenario 1 are strongly aligned with the actual values in both maneuvers. In the straight line maneuver, the estimates from Scenario 2 diverge completely, and the divergence behavior of the related algorithm can be noted in Fig. 7a. The estimated u from Scenario 3 are well converged to the actual values, whereas the estimated v has a constant bias. In the zigzag maneuver, a constant bias of the estimated v from Scenario 3 also exists, where a minor bias in the estimated u can also be seen. The estimates from Scenario 2 are similar to those from Scenario 1, except that larger errors occur when the heading switches in the labeled time steps in Fig. 7b. The algorithm diverges in these situations but will also converge after a considerable time period.

The results from Fig.7 indicate that constant biases of estimated v exist when γ is neglected in the CTRA. This can be explained by that v is highly sensitive to the vessel actual heading. It can be seen from Fig.2 that v does not exist if the vessel heading is aligned with the course vector. However, if the estimates of vessel heading are inaccurate due to, for example, the ignoring of projection error, this can lead to extra velocity components in the sway direction. Sway velocities are generally omitted in kinematic models with respect to ground vehicles, but can play a vital role in ship maneuvering and decision-making for

collision avoidance. A vessel with additional sway velocity can induce extra swept areas, and thus increase the risk of collision, contact, or near-miss accidents. Therefore, sway velocities must be included and precisely estimated for ship maneuvering.

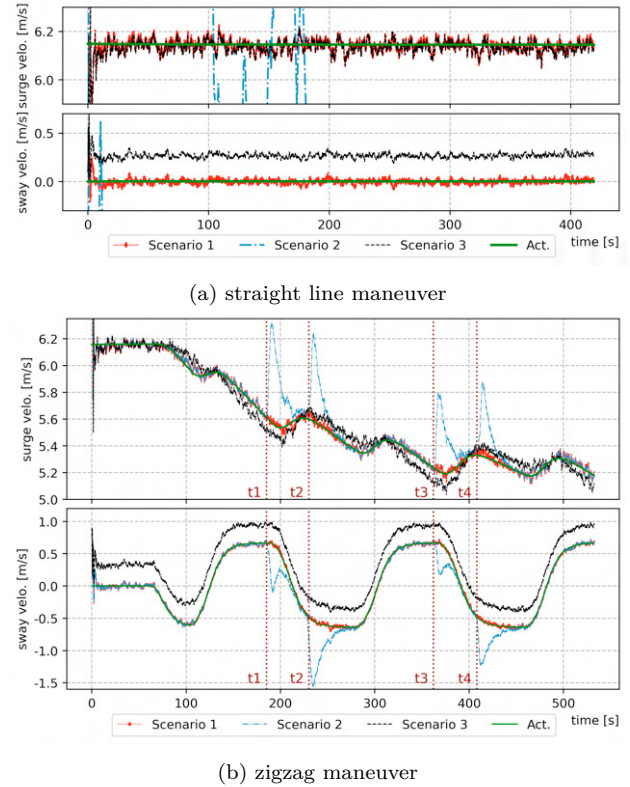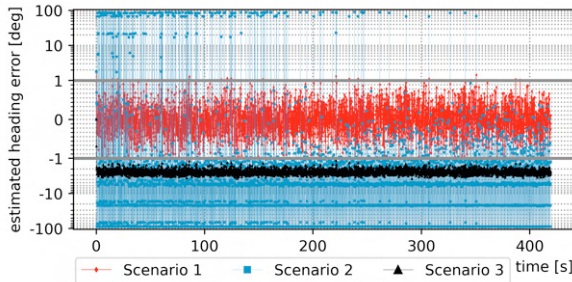(a) straight line maneuver

(b) zigzag maneuver

Fig. 7. The estimated surge and sway velocity

The evaluation of the estimated heading is based on the vector-based error representation (see Fig.3). It can be observed that the estimated heading from Scenario 2 becomes diverged when the vessel heading switches in both maneuvers. The estimated heading from Scenario 3 has a constant bias, and this is due to the reason that the grid convergence is not considered in this situation. One should note that the UKF without the switching correction is able to correct large estimation errors once the measured heading well behaves again. However, it takes a relatively long time for the positions and velocities to become converged, especially for the velocities under the same conditions. From this point of view, it can be considered that the switching correction also has a positive effect on the estimation accuracy of the positions and velocities in the CTRA. This is also attributed to the mathematical equations (14) that both positions and velocities are coupled with the heading. A heading innovation without the switching correction can corrupt the posterior estimates in the prediction step of the UKF. Since the UKF algorithm executes iteratively, these corrupted posterior estimates will be implemented in the next prediction step as the inputs to calculate the prior estimates. The uncorrected innovations of vessel heading hence spread to the position and velocity estimates.

The estimates of yaw rate and accelerations are summarized through the root mean square error (RMSE) in

(a) straight line maneuver
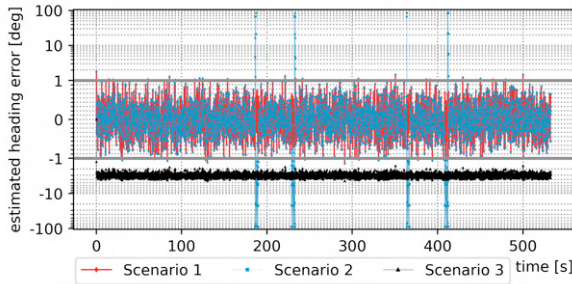
(b) zigzag maneuver

Fig. 8. Plots of proposed error for heading. Errors outside $[-1°, 1°]$ are plotted on log scale.

table 3 and table 4. The RMSEs of yaw rate and accelerations by all scenarios are similar to each other and have the same order of magnitude.

Table 3. RMSE in straight line maneuver

RMSE	Scenario 1	Scenario 2	Scenario 3
$r : [°/min]$	3.53×10^{-1}	3.56×10^{-1}	3.53×10^{-1}
$a_u : [m/s^2]$	4.85×10^{-2}	4.85×10^{-2}	4.85×10^{-2}
$a_v : [m/s^2]$	2.38×10^{-3}	2.39×10^{-3}	2.38×10^{-3}

Table 4. RMSE in zigzag maneuver

RMSE	Scenario 1	Scenario 2	Scenario 3
$r : [°/min]$	3.94×10^{-1}	3.94×10^{-1}	3.94×10^{-1}
$a_u : [m/s^2]$	4.81×10^{-3}	5.44×10^{-3}	6.09×10^{-3}
$a_v : [m/s^2]$	2.61×10^{-3}	3.70×10^{-3}	2.77×10^{-3}

6. CONCLUSIONS AND FUTURE WORK

The UTM projection can result in non-neglectable heading associated errors in high latitudes, and the switching of measured heading can cause significant inaccuracies in vessel state estimation. To mitigate these errors, two proposed solutions are introduced. As the innovative points, these methods consider the grid convergence that is embedded in the system and measurement model of the CTRA, and the correction of heading switching in the UKF. With these proposed methods, the UKF becomes more robust and can handle highly discontinuous measurements of vessel heading. By incorporating the correction made by the grid convergence, the estimation accuracy of vessel states in the CTRA can be further improved. As a result, these improvements can be applied to ship intelligence systems that support navigation safety in high-latitude areas. Future work involves conducting sea-trial experiments in the Tromsø area, which is also located in high latitudes.

REFERENCES

Aksenov, Y., Popova, E.E., Yool, A., Nurser, A.G., Williams, T.D., Bertino, L., and Bergh, J. (2017). On the future navigability of arctic sea routes: high-resolution projections of the arctic ocean and sea ice. *Marine Policy*, 75, 300–317.

Barrau, A. (2015). *Non-linear state error based extended Kalman filters with applications to navigation.* Thesis.

Kawase, K. (2012). Concise derivation of extensive coordinate conversion formulae in the gauss-krueger projection.

Kim, J.S., Lee, D.H., Kim, D.W., Park, H., Paik, K.J., and Kim, S. (2022). A numerical and experimental study on the obstacle collision avoidance system using a 2d lidar sensor for an autonomous surface vehicle. *Ocean Engineering*, 257, 111508. doi: https://doi.org/10.1016/j.oceaneng.2022.111508.

Li, X.R. and Jilkov, V.P. (2003). Survey of maneuvering target tracking. part i. dynamic models. *IEEE Transactions on Aerospace and Electronic Systems*, 39(4), 1333–1364.

Mu, X., He, B., Zhang, X., Song, Y., Shen, Y., and Feng, C. (2019). End-to-end navigation for autonomous underwater vehicle with hybrid recurrent neural networks. *Ocean Engineering*, 194, 106602. doi: https://doi.org/10.1016/j.oceaneng.2019.106602.

Munim, Z.H., Dushenko, M., Jimenez, V.J., Shakil, M.H., and Imset, M. (2020). Big data and artificial intelligence in the maritime industry: a bibliometric review and future research directions. *Maritime Policy & Management*, 47(5), 577–597. URL https://doi.org/10.1080/03088839.2020.1788731.

Osborne, P. (2013). *The Mercator Projections*. doi: 10.5281/zenodo.35392.

Perera, L.P. (2017). Navigation vector based ship maneuvering prediction. *Ocean Engineering*, 138, 151–160.

Philipp, B. (2009). Circstat: a matlab toolbox for circular statistics. *Journal of Statistical Software*, 31. doi: 10.18637/jss.v031.i10.

Takeno, M. and Katayama, T. (2012). A numerical method for continuous-discrete unscented kalman filter. *International Journal of Innovative Computing, Information and Control*, 8.

Wang, Y.F., Perera, L.P., and Batalden, B.M. (2022). The comparison of two kinematic motion models for shipping maneuvers (79583). In *The 42nd International Conference on Ocean, Offshore and Arctic Engineering (OMAE)*.

Zhang, Z.Q., Meng, X.L., and Wu, J.K. (2012). Quaternion-based kalman filter with vector selection for accurate orientation tracking. *IEEE Transactions on Instrumentation and Measurement*, 61(10), 2817–2824.